

SVMA: A GAN-based model for Monocular 3D Human Pose Estimation

Yicheng Deng
Beijing Jiaotong University
ycdeng@bjtu.edu.cn

Yongqi Sun
Beijing Jiaotong University
yqsun@bjtu.edu.cn

Jiahui Zhu
Beijing Jiaotong University
jhzhu@bjtu.edu.cn

Abstract

Recovering 3D human pose from 2D joints is a highly unconstrained problem, especially without any video or multi-view information. We present an unsupervised GAN-based model to recover 3D human pose from 2D joint locations extracted from a single image. Our model uses a GAN to learn the mapping of distribution from 2D poses to 3D poses, not the simple 2D-3D correspondence. Considering the reprojection constraint, our model can estimate the camera so that we can reproject the estimated 3D pose to the original 2D pose. Based on this reprojection method, we can rotate and reproject the generated pose to get our "new" 2D pose and then use a weight sharing generator to estimate the "new" 3D pose and a "new" camera. Through the above estimation process, we can define the single-view-multi-angle consistency loss during training to simulate multi-view consistency, which means the 3D poses and cameras estimated from two angles of a single view should be able to be mixed to generate rich 2D reprojections, and the 2D reprojections reprojected from the same 3D pose should be consistent. The experimental results on Human3.6M show that our method outperforms all the state-of-the-art methods, and results on MPI-INF-3DHP show that our method outperforms state-of-the-art by approximately 15.0%.

1. Introduction

3D human pose estimation from monocular images has always been a problem in computer vision[2][10] with numerous applications such as motion recognition, virtual reality, and human-computer interaction. Although some current deep learning methods have achieved good results by directly recovering 2d to 3d[7][19][22], they usually cannot avoid the problem of overfitting. That is, it is difficult to estimate unknown poses and camera positions. Not only that, there are currently fewer datasets with 3D annotations, especially for pose datasets in the wild, which is extremely difficult to perform 3D annotation work, making unsupervised learning for 3D human pose estimation is of great significance. However, this is still a difficult problem.

To solve the above two problems, we propose an unsupervised adversarial training method for 3D human pose and camera estimation. We use a GAN to learn a distribution of 3D human poses. First, we set up a generator to estimate a 3D pose and a camera simultaneously from an input 2D pose, and then we can reproject the estimated 3D pose to get the corresponding 2D pose.

Recently, there are several methods that use multi-view data and achieve good results[18][34], but setting up multi-view cameras in the wild is also extremely difficult. We solve this problem by simulating multi-view consistency based on a single image. We use two networks with shared weights to impose our single-view-multi-angle consistency to simulate multi-view consistency: if the estimated 3D human pose is accurate enough, then our 3D pose is rotated at a random angle, we can still get a reasonable "new" 2D pose by reprojecting the rotated 3D pose using the estimated camera, and then we pass the "new" 2D pose through the weight sharing generator to get the "new" 3D pose and the corresponding camera. Since the whole process is performed from the same view, the two cameras we estimate should be the same, and then we have our SVMA consistency loss, which will be described in detail in section 3. In addition to the generator, we also introduce a discriminator, whose input is our reprojected 2D pose or a 2D pose sampled from the real distribution, to determine whether our reprojected pose is from the real pose distribution, finally make our generator learn the mapping of distribution from 2D poses to 3D poses, not a simple 2D-3D correspondence.

To prove the effectiveness of our method, we perform experiments on four datasets Human3.6M[13], MPI-INF-3DHP[23], MPII[1], and Leed Sports Pose(LSP)[14]. Both the quantitative and qualitative experimental results show our method outperforms state-of-the-art methods. The model trained on a specific dataset can also get good results on other datasets, which shows our method can effectively avoid the problem of overfitting.

Our contributions are as follows:

- We present SVMA model: an unsupervised adversarial training method to learn a 3D human pose from a 2D pose in a single image without any requiring 3D data.

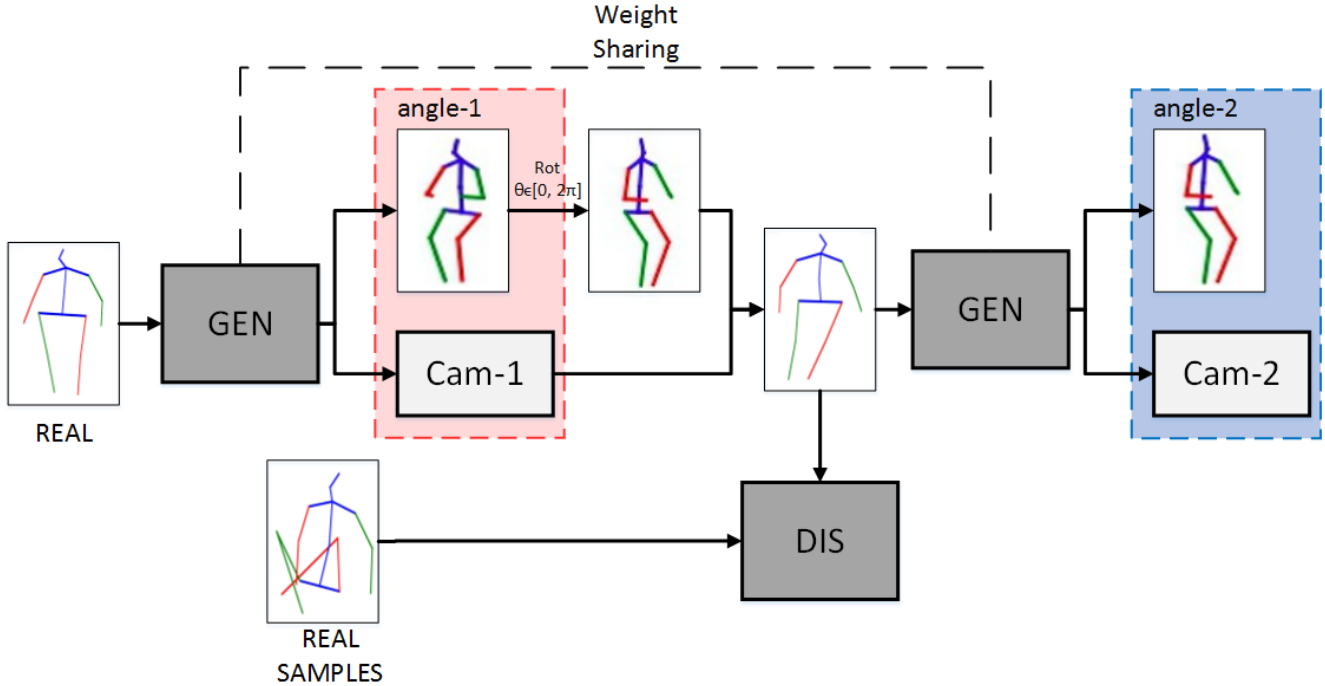


Figure 1. The main structure of our proposed adversarial training framework. Our generator predicts a 3D pose and a camera which is used to project the 3D pose back to 2D. We rotate the estimated 3D pose and project the rotated 3D pose back to 2D. The 2D reprojection or a real 2D pose is fed to a discriminator for discrimination. We also employ a weight sharing generator to lift the 2D reprojection again, allowing the network to impose SVMA consistency constraint.

- Our method is the first unsupervised method that simultaneously estimates a 3D pose and a camera from a single image.
- Our method simulates multi-view consistency by using two weight sharing networks to impose single-view-multi-angle consistency constraint, which enriches supervision information.
- Our method is tested on multiple datasets to prove the effectiveness of estimating unknown 3D human poses and cameras.

2. Related work

Fully Supervised Methods Recently, several methods make full use of both 2D and 3D ground truth based on large datasets which contain millions of images with corresponding 3D pose annotations. Madadi et al.[21] use CNN-based 3D joint predictions to regress SMPL pose and shape parameters and then use these parameters to get the estimated 3D pose. Sun et al.[30] propose an end-to-end model to regress a 3D human pose from 2D heat maps. Dushyant et al.[24] propose a CNN-based model, which regresses 2D and 3D joint coordinates and motion skeleton to produce a real-time stable 3D reconstruction of

motion. The above methods are called end-to-end methods. In addition to these methods, there are also some methods divided into two stages. The first stage is to perform 2D pose detection on a single image and predict its 2D joint coordinates[4][5][6][25][26][29][31]; the second stage is predicting 3D joint coordinates from the 2D joint coordinates through regression analysis or model fitting[16][19][22][33]. Recently, some methods have been proposed for the second stage of the two-stage method, and these methods aim to learn the 2D-3D correspondence with the given paired 2D and 3D data. Martinez et al.[22] propose a simple but effective regression network to estimate a 3D human pose directly from a 2D pose, and this method is considered to be the baseline due to its simplicity and high precision estimation. Hossain et al.[11] extend the baseline method by employing a recurrent neural network for a human pose sequence. Although these methods have achieved outstanding results, they need a lot of data with 3D annotations, and they can only be generalized to similar datasets.

Weakly Supervised Methods Weakly supervised methods only require limited 3D annotations or an unpaired 2D-3D correspondence. Zhou et al.[38] propose a two-stage transfer model to generate 2D heat maps and regress the joint depths. Yang et al.[37] propose an adversarial training method based on multiple representations. They use a

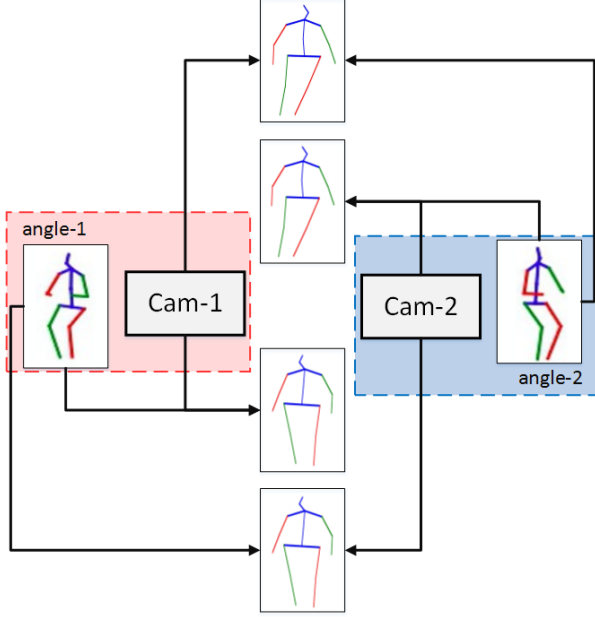


Figure 2. The estimated 3D poses and cameras from different angles can be mixed to generate rich 2D reprojections. The 2D reprojections from the same angle should be the same.

discriminator to evaluate results by RGB images, geometric representations, and heat maps. Considering the reprojection constraint, Wandt et al.[33] propose a GAN-based model named RepNet to estimate a 3D pose and a camera simultaneously and use a discriminator to evaluate the estimated 3D pose and the corresponding KCS matrix. Deng et al.[8] propose an adversarial training method that considers 3D information and 2D information simultaneously and trains the 2D-3D lifter, reprojection network, and discriminator synchronously. Although these methods somehow solve the problem of overfitting, they still require 3D annotation data, whose acquisition is time-consuming and labor-intensive.

Unsupervised Methods Unsupervised methods make full use of images or 2D data, and they don't require any 3D annotation. Rhodin et al.[27] propose an encoder-decoder to perform 3D human pose estimation based on unsupervised geometry-aware representations. Their method requires multi-view 2D data to learn the appearance representation. Kudo et al.[19] propose an unsupervised method to perform 3D human pose estimation. They randomly rotate an estimated 3D pose and then reproject it back to 2D and use a discriminator to evaluate the 2D reprojection. Chen et al.[7] propose an unsupervised method to estimate a 3D pose. Half of their model is similar to [19], and the other half of their model lifts the 2D reprojection to a 3D pose again and reprojects the 3D pose back to 2D once more. Kocabas et al.[18] propose a multi-view self-supervised method. They use traditional methods to gen-

erate a 3D pose using multi-view 2D poses and use it as self-supervised information. Kundu et al.[20] propose a differentiable and modular self-supervised method for 3D human pose estimation along with the discovery of 2D part segments from unlabeled video frames.

However, their methods can't be generalized to unknown motions and camera positions well. In this paper, we propose an unsupervised adversarial training method to estimate a 3D human pose and a camera simultaneously. We also use two networks with shared weights to simulate multi-view consistency to impose a single-view-multi-angle consistency constraint.

3. Method

In this section, we introduce our unsupervised method to lift 2D joint locations to 3D poses in the following relative 3D space (XYZ coordinates). First, we take the hip joint as the root joint to align all 2D and 3D pose coordinates. In addition, we use the data preprocessing method introduced in section 3.1 to further process the aligned 2d and 3d coordinates.

3.1. Data preprocessing

Let $x_{real} \in \mathbb{R}^{2N} = (x_1, y_1, x_2, y_2, \dots, x_N, y_N)$ be 2D joint locations and $X_{real} \in \mathbb{R}^{3N} = (X_1, Y_1, Z_1, X_2, Y_2, Z_2, \dots, X_N, Y_N, Z_N)$ be real 3D poses, where N represents the number of human joints. We assume a perspective camera, so we have

$$x_i = f * X_i / Z_i, i = 1, 2, \dots, N, \quad (1)$$

$$y_i = f * Y_i / Z_i, i = 1, 2, \dots, N, \quad (2)$$

where f is the focal length of the camera. We assume the f of the camera is 1. So we have

$$x_i = X_i / Z_i, i = 1, 2, \dots, N, \quad (3)$$

$$y_i = Y_i / Z_i, i = 1, 2, \dots, N. \quad (4)$$

And we assume that the distance from the camera to the 3D skeleton is $d = 10$. So we have the data preprocessing method based on the triangle similarity principle. We preprocess 2D joint locations so that the average distance from other joints to the root joint (i.e., hip joint) is $1/d$. We preprocess the 3D poses that are not used in the training process so that the average distance from the other joints to the root joint is 1.

3.2. Generator

The input of our generator is x_{real} , and the generator is divided into two parts. pose estimation part and camera estimation part. The output of the pose estimation part is D , from the output we have $Z = D + d$, from Z and the equations (3) and (4) we have $X_{pred} = (X, Y, Z)$. To impose

SVMA consistency constraint, we also estimate a more simplified weak perspective camera. The output of the camera estimation part is the weak perspective camera that is a 6-dimensional vector, we reshape it to $K \in \mathbb{R}^{2*3}$.

For the network structure of our generator, we first use a shared residual block to extract the feature of input 2D joint locations. Then, for the pose estimation part, we add two residual blocks after the shared residual block and finally add a fully connected layer to output a $3N$ -dimensional vector. And for the camera estimation part, we add two residual blocks after the shared residual block and finally add a fully connected layer to output a 6-dimensional vector. In addition, there are batch-normalization[12], Leaky-Relu[3], and dropout[28] after each layer.

3.3. Single-View-Multi-Angle consistency

After we get the estimated 3D pose X_{pred} from angle-1, we rotate it around the y -axis by θ radian which is obtained from a uniform distribution on $[0, 2\pi]$, and then we have the rotated 3D pose

$$\tilde{X}_{pred} = (X_{pred} - [0, 0, d]) \begin{bmatrix} \cos\theta & 0 & -\sin\theta \\ 0 & 1 & 0 \\ \sin\theta & 0 & \cos\theta \end{bmatrix} + [0, 0, d], \quad (5)$$

which is from angle-2. Through \tilde{X}_{pred} and the estimated camera K we have the rotated 2D reprojection

$$\tilde{x}_{proj} = K \tilde{X}_{pred}. \quad (6)$$

Then we pass \tilde{x}_{proj} through a weight sharing generator again. Then through the same data processing method, $\tilde{X}_{rot.pred}$ and camera \tilde{K} from angle-2 can be obtained. $\tilde{X}_{rot.pred}$ and \tilde{X}_{pred} should be the same. So we have

$$\mathcal{L}_{3D} = \frac{1}{N} \left\| \tilde{X}_{rot.pred} - \tilde{X}_{pred} \right\|_2, \quad (7)$$

where $\|\cdot\|_2$ represents the 2-norm.

Because the two angles involved in the whole estimation are from the single view, \tilde{K} and K should also be the same. So we have

$$\mathcal{L}_{eq} = \frac{1}{6} \left\| K - \tilde{K} \right\|_1, \quad (8)$$

where $\|\cdot\|_1$ represents the 1-norm. From this, we have our single-view-multi-angle consistency loss, as shown in the figure 2, which means our two estimated 3D poses X_{pred} and $\tilde{X}_{rot.pred}$, and our two estimated cameras K and \tilde{K} can be mixed to generate four 2D reprojections. Then we enforce single-view-multi-angle consistency to simulate multi-view consistency

$$\mathcal{L}_{svma} = \frac{1}{mN} \sum_{i,j=1,i<j}^m \|P_i - P_j\|_2 + \frac{1}{nN} \sum_{i,j=1,i<j}^n \|\tilde{P}_i - \tilde{P}_j\|_2, \quad (9)$$

where m is the number of 2D reprojections or ground truth from angle-1 and n is the number of 2D reprojections from angle-2. P_i and P_j represent 2D reprojections from angle-1, \tilde{P}_i and \tilde{P}_j represent the i -th and j -th 2D reprojections from angle-2.

3.4. Discriminator

To enhance the performance of our generator, we introduce a discriminator to determine the reality of the generated 3D pose and finally make the generator learn the mapping of the distribution from 2D poses to 3D poses instead of a simple one-to-one correspondence. The input of our discriminator is the rotated 2D reprojection \tilde{x}_{proj} or the 2D pose sampled from real samples x_{sam} . Note that \tilde{x}_{proj} and x_{sam} are not the same. The output is a probability, which represents the probability that the current input is from real distribution.

The network structure of our discriminator includes a fully connected layer to upgrade the input, followed by two residual blocks, and a fully connected layer to reduce the dimensionality to get the output, where Leaky-Relu follows each network layer.

3.5. Loss functions

For our GAN, the standard WGAN-gp loss function is used.

$$\min_{\theta_G} \max_{\theta_D} \mathcal{L}_{adv} = \mathbb{E}(D(\tilde{x}_{proj})) - \mathbb{E}(D(x_{sam})) + \lambda_{gp} (\nabla_{\hat{x}}(D(\hat{x}) - 1)), \quad (10)$$

where \hat{x} represent the linear combination of x_{sam} and \tilde{x}_{proj} .

Like [33], we have loss of the camera, the estimated camera K should satisfy

$$K K^T = s^2 I_2, \quad (11)$$

where s is the scale of the projection and I_2 is the 2*2 identity matrix. Because s equals to the largest singular value (or the l_2 -norm) of K . Both singular values are equal. Since the trace of $K K^T$ is the sum of the squared singular values

$$s = \sqrt{\text{trace}(K K^T)/2}, \quad (12)$$

so we have camera loss function

$$\mathcal{L}_{cam} = \left\| \frac{2}{\text{trace}(K K^T)} K K^T - I_2 \right\|_F + \mathcal{L}_{eq}, \quad (13)$$

where $\|\cdot\|_F$ represents the Frobenius norm.

In addition, we consider the constraint of the bone length of the human body. There are several pairs of bones B in the human body that have a symmetrical relationship in length in the dataset. So we have our symmetric loss

$$\mathcal{L}_{sym} = \frac{1}{q} \sum_i^q \|B_i - B'_i\|_2^2, \quad (14)$$

where q is the number of pairs of bones that have a symmetrical relationship, B_i and B'_i are the i -th pair of two bones with a symmetrical relationship.

Then, we impose another constraint L_{angle} , which guarantees that the z -components of the generated 3D pose will not be inverted, by referring to Yasunori[19]. Similarly, we define the face orientation vector $v = [v_x, v_y, v_z] = j_{nose} - j_{neck} \in \mathbb{R}^3$ and shoulder orientation vector $w = [w_x, w_y, w_z] = j_{ls} - j_{rs} \in \mathbb{R}^3$, where $j_{nose}, j_{neck}, j_{ls}, j_{rs} \in \mathbb{R}^3$ represent the 3D coordinates of the nose, neck, left shoulder and right shoulder respectively. According to the above mentioned constraints, the angle β between v and w on the $z - x$ plane should satisfy

$$\sin \beta = \frac{v_z w_x - v_x w_z}{\|v\| \|w\|} \geq 0. \quad (15)$$

To satisfy this inequality, let

$$\mathcal{L}_{angle} = \max(0, -\sin \beta) = \max(0, \frac{v_x w_z - v_z w_x}{\|v\| \|w\|}). \quad (16)$$

Finally, through equations (7), (8), (9), (13), (14), and (16), we obtain the final loss function of the generator as follows:

$$\mathcal{L} = \mathcal{L}_{adv} + \lambda_1 \mathcal{L}_{angle} + \lambda_2 \mathcal{L}_{cam} + \lambda_3 \mathcal{L}_{sym} + \lambda_4 \mathcal{L}_{3D} + \lambda_5 \mathcal{L}_{svma}, \quad (17)$$

where $\lambda_1, \lambda_2, \lambda_3, \lambda_4$, and λ_5 represent the weight coefficients of the loss terms $L_{angle}, L_{cam}, L_{sym}, L_{3D}, L_{svma}$, respectively.

3.6. Training details

As mentioned above, we use the standard WGAN-GP loss function and some other loss functions to train our GAN. We use Adam optimizer[17] for both two networks with a learning rate of $5.5e-5$, $\beta_{1} = 0.7$ and $\beta_{2} = 0.9$. The loss weights are set as $\lambda_1=1, \lambda_2=1, \lambda_3=0.01, \lambda_4=0.1$, and $\lambda_5=10$.

4. Experiments and results

We evaluated our model on the Human3.6M[13], MPI-INF-3DHP[23] datasets and showed quantitative results. In addition, we also show qualitative results on the in-the-wild datasets MPII[1] and LSP[14], where 3D ground truth data is not available.

4.1. Datasets and metrics

Human3.6M This is one of the largest 3D human pose datasets, consisting of 3.6 million 3D human poses. The dataset contains video and MoCap data captured from 4 different viewpoints from 11 subjects performing typical activities such as directing, walking, sitting, etc. We evaluate the

Table 1. The results of 3D human pose estimation on the Human 3.6M dataset. GT denotes the input 2D joint locations are ground truth and IMG denotes the input 2D joint locations are from 2D detector. (†) denotes the method uses temporal information, (+) denotes the method uses extra data for training.

Type	Methods	GT	IMG
Full	HMR[15]	56.8/58.1	-
	Martinez et al.[22]	37.1	52.1
Weak	3DInterpreter[35]	88.6	98.4
	AIGN[9]	79.0	97.2
	HMR[15]	66.5	-
	RepNet[33]	38.2	65.1
Unsupervised	Kudo et al.[19]	130.9	173.2
	Chen et al.[7](†)(+)	51.0	68.0
	Chen et al.[7]	58.0	-
	Kundu et al.[20]	62.4	99.2
	Ours	56.8	98.3
	Ours(SH/GT)	-	64.8

accuracy of pose estimation in terms of MPJPE(mean per joint position error) in millimeters after scaling and rigid alignment on the ground truth skeleton, i.e., P-MPJPE. We train our model on subjects S1, S5, S6, S7, S8 and evaluate on subjects S9, S11.

MPI-INF-3DHP The MPI-INF-3DHP is a large human pose dataset consists of 3D data captures using a marker-less multi-camera MoCap system. The dataset has eight actors performing several actions, which are more diverse than the Human 3.6M dataset. Data contains both indoor and outdoor scenes. We evaluate valid images from the test-set containing 2929 frames following [15] and report P-MPJPE, Percentage of Correct Keypoints (PCK) @150mm, and Area Under the Curve(AUC) computed for a range of PCK thresholds. PCK and AUC include the results of using and not using rigid alignment.

4.2. Quantitative Results

Results on Human 3.6M Table 1 shows the results on Human 3.6M. The lower the P-MPJPE value is, the better the model performances. In addition to comparing with the state-of-the-art unsupervised 3D pose estimation method of Kundu et al. and Chen et al.[7], we also show results from fully supervised and weakly supervised methods. Results show that our method outperforms state-of-the-art unsupervised methods and several weakly supervised methods. We also show the results obtained by training on 2D locations detected by stacked hourglass and testing on 2D ground truth. The results indicate that our model works well for estimating the depth of human poses. Figure 3 shows some reconstruction examples on the Human3.6M dataset. Our method can be estimated very well for even more complicated actions from these reconstruction results, but our method cannot be reconstructed very well for some special angles.

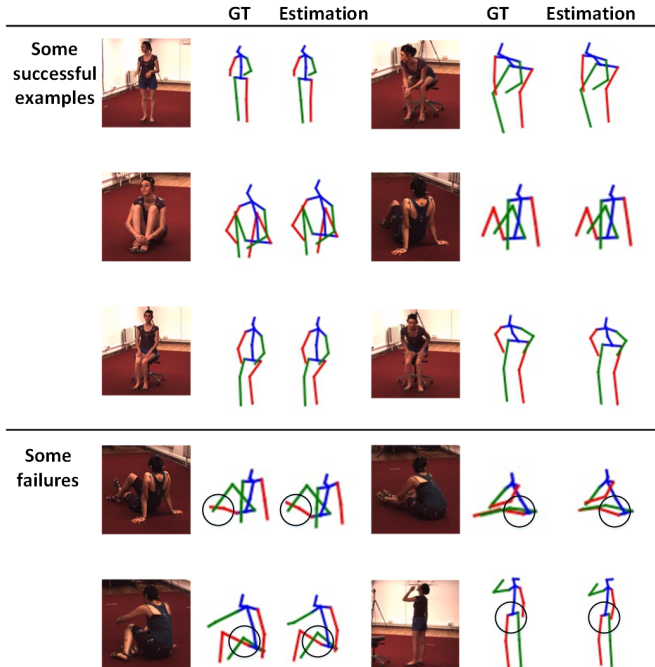


Figure 3. Qualitative results on Human 3.6M dataset. The first three rows are some examples of successful reconstruction, the last two lines are some examples of failed reconstruction.

Results on MPI-INF-3DHP Table 2 and Table 3 show the results on MPI-INF-3DHP. A higher value is better for PCK and AUC. Our results show our method outperforms state-of-the-art by 15.0% in P-MPJPE with training on MPI-INF-3DHP and 21.0% in P-MPJPE with training on Human 3.6M. Our method is even better than some methods that use multi-view data or temporal data and extra data on training. Hence, our experimental results show that our model can be applied to multiple datasets and achieves better performance in human pose estimation. There is only a minor improvement of the AUC and P-MPJPE and even a minor deterioration of the PCK compared to the model trained on Human3.6M. The above results indicate that our model converges to a similar distribution of feasible human poses for both training sets, which means that our method can be well generalized to unseen data.

Ablation Study We also conduct ablation studies to evaluate the effectiveness of the adversarial training and our SVMA consistency loss. The results are shown in Table 4. 'without Dis' represents our experimental results when we train our model without using a discriminator. 'without SVMA' represents our experimental results when we train our model without using SVMA consistency loss, which means we input 2D joint locations through the generator only one time. The results show that our SVMA consistency loss further improves the performance of our model by 20%, which can help our generator generate more plau-

Table 2. The results of 3D human pose estimation on the MPI-INF-3DHP dataset (without using a scaling and rigid alignment). (†) denotes the method uses temporal information, (‡) denotes the method uses multi-view information, (+) denotes the method uses extra data for training.

Supervision	Methods	Training Data	Absolute	
			PCK	AUC
Full	VNect[24]	H36M+MPI	76.6	40.4
	Mehta[23]	MPI	72.5	36.9
	Mehta[23]	H36M	64.7	31.7
Weak	SPIN[35]	Various	66.8	30.2
	HMR[15]	H36M+MPI	59.6	27.9
Unsupervised	Chen et al.[7](†)(+)	H36M	64.3	31.6
	Chen et al.[7](†)(+)	MPI	71.1	36.3
	Epipolar[18](‡)	MPI	64.7	-
	Ours	H36M	64.8	31.6
	Ours	MPI	66.5	33.0

Table 3. The results of 3D human pose estimation on the MPI-INF-3DHP dataset (using a scaling and rigid alignment).

Supervision	Methods	Training Data	Rigid Alignment		
			PCK	AUC	P-MPJPE
Full	VNect[24]	H36M+MPI	83.9	47.3	98.0
	DenseRac[36]	H36M+MPI	86.3	47.8	89.8
Weak	SPIN[35]	Various	87.0	48.5	80.4
	HMR[15]	H36M+MPI	77.1	40.7	113.2
Unsupervised	PoseNet3D[32]	H36M	81.9	43.2	102.4
	Kundu et al.[20]	H36M	82.1	56.3	103.8
	Kundu et al.[20]	MPI	84.6	60.8	93.9
	Ours	H36M	86.8	51.2	80.9
	Ours	MPI	86.6	53.1	79.8

Table 4. Ablation Studies.

Methods	P-MPJPE	
	Human 3.6M	MPI-INF-3DHP
without Dis	90.0	134.2
without SVMA	70.9	98.7
All equipped	56.8	79.8

sible 3D poses and cameras.

4.3. Qualitative Results

To show the generalization of our model, we conduct experiments on MPII and LSP datasets without being trained on them but trained on Human 3.6M, and show some examples of estimated 3D poses in Figure. It can be seen that our model performs well with standard 2D pose datasets, which contains more complicated in-the-wild poses.

5. Conclusion

For 3D human pose estimation, the acquisition of 3D annotation data is time-consuming and expensive, which is still a difficult problem. We present the SVMA model: an unsupervised GAN-based model to estimate a 3D pose and a camera simultaneously through a 2D pose without any other data. Considering the 3D poses and cameras estimated from two angles from the single view should be able to be mixed to generate rich 2D projections and the 2D pro-



Figure 4. Some examples of reconstruction on the MPII dataset. The left is the image and the right is the corresponding reconstructed 3D pose.

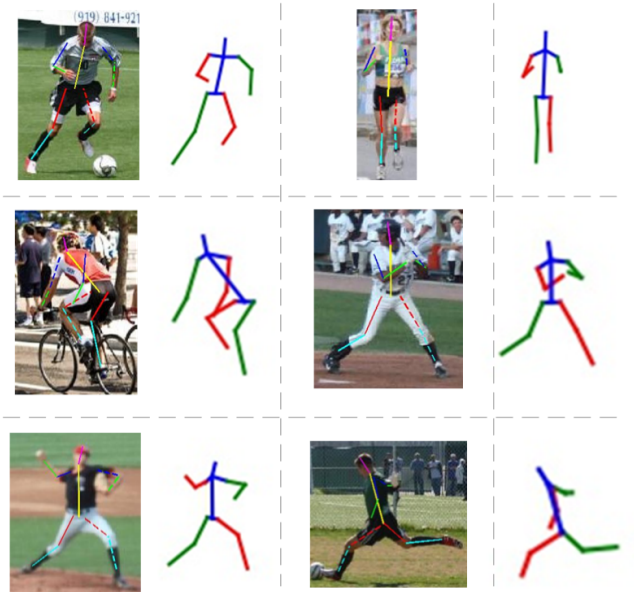


Figure 5. Some examples of reconstruction on the LSP dataset. The left is the image and the 2D pose overlaid on the image, the right is the corresponding reconstructed 3D pose.

jections reprojected from the same 3D pose should be consistent, we use two networks with shared weights to simulate multi-view consistency to impose reprojection constraint and single-view-multi-angle consistency constraint without any multi-view data. The experimental results show that our method outperforms the state-of-the-art methods by

2.0% on Human 3.6M and 15.0% on MPI-INF-3DHP. We also conduct qualitative experiments on MPII and LSP to show the generalization of our method. In the future, we plan to improve the model’s performance by applying it to videos.

References

- [1] M. Andriluka, L. Pishchulin, P. Gehler, and B. Schiele. Human pose estimation: New benchmark and state of the art analysis. In *Computer Vision and Pattern Recognition (CVPR)*, 2014. 1, 5
- [2] O. Arıkan, L. Ikemoto, and D. A. Forsyth. Computational studies of human motion: Tracking and motion synthesis. *Now Publishers Inc*, 2006. 1
- [3] B Xu, N Wang, T Chen, M Li. Empirical evaluation of rectified activations in convolutional network. 2015. 4
- [4] A. Bulat and G. Tzimiropoulos. Human pose estimation via convolutional part heatmap regression. In *European Conference on Computer Vision*, 2016. 2
- [5] Z. Cao, T. Simon, S. E. Wei, and Y. Sheikh. Realtime multi-person 2d pose estimation using part affinity fields. In *2017 IEEE Conference on Computer Vision and Pattern Recognition (CVPR)*, 2017. 2
- [6] J. Carreira, P. Agrawal, K. Fragkiadaki, and J. Malik. Human Pose Estimation with Iterative Error Feedback. In *2016 IEEE Conference on Computer Vision and Pattern Recognition (CVPR)*, pages 4733–4742, Las Vegas, NV, USA, June 2016. IEEE. 2
- [7] C. H. Chen, A. Tyagi, A. Agrawal, D. Drover, M. V. Rohith, S. Stojanov, and J. M. Rehg. Unsupervised 3d pose estimation with geometric self-supervision. In *2019 IEEE/CVF Conference on Computer Vision and Pattern Recognition (CVPR)*, 2020. 1, 3, 5, 6
- [8] Y. Deng, C. Sun, Y. Sun, and J. Zhu. A synchronized reprojection-based model for 3d human pose estimation. *arXiv, preprint arXiv:2106.04274*, 2021. 3
- [9] H.-Y. Fish Tung, A. W. Harley, W. Seto, and K. Fragkiadaki. Adversarial inverse graphics networks: Learning 2d-to-3d lifting and image-to-image translation from unpaired supervision. In *Proceedings of the IEEE International Conference on Computer Vision (ICCV)*, Oct 2017. 5
- [10] D. Hogg. Model-based vision: A program to see a walking person. *Image and Vision Computing*, 1(1):5–20, 1983. 1
- [11] M. Hossain and J. J. Little. Exploiting temporal information for 3d pose estimation. In *European Conference on Computer Vision (ECCV)*, 2018. 2
- [12] S. Ioffe and C. Szegedy. Batch normalization: Accelerating deep network training by reducing internal covariate shift. In *ICML*, 2015. 4
- [13] C. Ionescu, D. Papava, V. Olaru, and C. Sminchisescu. Human3.6m: Large scale datasets and predictive methods for 3d human sensing in natural environments. *IEEE Transactions on Pattern Analysis and Machine Intelligence*, 36(7):1325–1339, 2014. 1, 5
- [14] S. Johnson and M. Everingham. Clustered pose and nonlinear appearance models for human pose estimation. In *British Machine Vision Conference*, 2010. 1, 5

- [15] A. Kanazawa, M. J. Black, D. W. Jacobs, and J. Malik. End-to-end recovery of human shape and pose. In *2018 IEEE/CVF Conference on Computer Vision and Pattern Recognition*, 2018. 5, 6
- [16] Y. Kim and D. Kim. A cnn-based 3d human pose estimation based on projection of depth and ridge data. *Pattern Recognition*, 106:107462, 2020. 2
- [17] D. Kingma and J. Ba. Adam: A method for stochastic optimization. *Computer Science*, 2014. 5
- [18] M. Kocabas, S. Karagoz, and E. Akbas. Self-supervised learning of 3d human pose using multi-view geometry. In *2019 IEEE/CVF Conference on Computer Vision and Pattern Recognition (CVPR)*, 2019. 1, 3, 6
- [19] Y. Kudo, K. Ogaki, Y. Matsui, and Y. Odagiri. Unsupervised adversarial learning of 3d human pose from 2d joint locations. *arXiv preprint arXiv: 1803.08244*, 2018. 1, 2, 3, 5
- [20] J. Kundu, S. Seth, V. Jampani, M. Rakesh, R. Babu, and A. Chakraborty. Self-supervised 3d human pose estimation via part guided novel image synthesis. In *Proceedings of the IEEE/CVF Conference on Computer Vision and Pattern Recognition (CVPR)*, pages 6151–6161, June 2020. 3, 5, 6
- [21] M. Madadi, H. Bertiche, and S. Escalera. Smplr: Deep learning based smpl reverse for 3d human pose and shape recovery. *Pattern Recognition*, 106:107472, 2020. 2
- [22] J. Martinez, R. Hossain, J. Romero, and J. J. Little. A simple yet effective baseline for 3d human pose estimation. In *2017 IEEE International Conference on Computer Vision (ICCV)*, 2017. 1, 2, 5
- [23] D. Mehta, H. Rhodin, D. Casas, P. Fua, O. Sotnychenko, W. Xu, and C. Theobalt. Monocular 3d human pose estimation in the wild using improved cnn supervision. In *3D Vision(3DV)*, 2017. 1, 5, 6
- [24] D. Mehta, S. Sridhar, O. Sotnychenko, H. Rhodin, and C. Theobalt. Vnect: Real-time 3d human pose estimation with a single rgb camera. *ACM Transactions on Graphics*, 36(4), 2017. 2, 6
- [25] A. Newell, K. Yang, and J. Deng. Stacked hourglass networks for human pose estimation. In *ECCV*, 2016. 2
- [26] L. Pishchulin, E. Insafutdinov, S. Tang, B. Andres, M. Andriluka, P. Gehler, and B. Schiele. Deepcut: Joint subset partition and labeling for multi person pose estimation. In *Computer Vision and Pattern Recognition*, 2016. 2
- [27] H. Rhodin, M. Salzmann, and P. Fua. Unsupervised geometry-aware representation for 3d human pose estimation. In *European Conference on Computer Vision*, 2018. 3
- [28] N. Srivastava, G. Hinton, A. Krizhevsky, I. Sutskever, and R. Salakhutdinov. Dropout: A simple way to prevent neural networks from overfitting. *Journal of Machine Learning Research*, 15(1):1929–1958, 2014. 4
- [29] K. Sun, B. Xiao, D. Liu, and J. Wang. Deep high-resolution representation learning for human pose estimation. In *2019 IEEE/CVF Conference on Computer Vision and Pattern Recognition (CVPR)*, 2019. 2
- [30] X. Sun, B. Xiao, F. Wei, S. Liang, and Y. Wei. Integral Human Pose Regression. In V. Ferrari, M. Hebert, C. Sminchisescu, and Y. Weiss, editors, *Computer Vision – ECCV 2018*, volume 11210, pages 536–553. Springer International Publishing, Cham, 2018. Series Title: Lecture Notes in Computer Science. 2
- [31] A. Toshev and C. Szegedy. DeepPose: Human Pose Estimation via Deep Neural Networks. In *2014 IEEE Conference on Computer Vision and Pattern Recognition*, pages 1653–1660, Columbus, OH, USA, June 2014. IEEE. 2
- [32] S. Tripathi, S. Ranade, A. Tyagi, and A. Agrawal. PoseNet3d: Learning temporally consistent 3d human pose via knowledge distillation. In *2020 International Conference on 3D Vision (3DV)*, pages 311–321, 2020. 6
- [33] B. Wandt and B. Rosenhahn. Repnet: Weakly supervised training of an adversarial reprojection network for 3d human pose estimation. *IEEE Conf. Computer Vision and Pattern Recognition (CVPR)*, 2019. 2, 3, 4, 5
- [34] B. Wandt, M. Rudolph, P. Zell, H. Rhodin, and B. Rosenhahn. Canonpose: Self-supervised monocular 3d human pose estimation in the wild. In *Computer Vision and Pattern Recognition (CVPR)*, 2021. 1
- [35] J. Wu, T. Xue, J. J. Lim, Y. Tian, J. B. Tenenbaum, A. Torralba, and W. T. Freeman. Single image 3d interpreter network. In *ECCV*, 2016. 5, 6
- [36] Y. Xu, S. C. Zhu, and T. Tung. Denserac: Joint 3d pose and shape estimation by dense render-and-compare. In *2019 IEEE/CVF International Conference on Computer Vision (ICCV)*, 2020. 6
- [37] W. Yang, W. Ouyang, X. Wang, J. Ren, H. Li, and X. Wang. 3D Human Pose Estimation in the Wild by Adversarial Learning. In *2018 IEEE/CVF Conference on Computer Vision and Pattern Recognition*, pages 5255–5264, Salt Lake City, UT, USA, June 2018. IEEE. 2
- [38] X. Zhou, Q. Huang, X. Sun, X. Xue, and Y. Wei. Towards 3d human pose estimation in the wild: a weakly-supervised approach. In *2017 IEEE International Conference on Computer Vision (ICCV)*, 2017. 2